Evaluation of threading dislocation densities in In- and N-face InN

C. S. Gallinat,[a] G. Koblmüller, Feng Wu, and J. S. Speck
Materials Department, University of California Santa Barbara, California 93106-5050, USA

(Received 8 October 2009; accepted 19 January 2010; published online 8 March 2010)

The threading dislocation (TD) structure and density has been studied in In- and N-face InN films grown on GaN by plasma-assisted molecular beam epitaxy. The TD densities were determined by nondestructive x-ray diffraction rocking curve measurements in on-axis symmetric and off-axis skew symmetric geometries and calibrated by transmission electron microscopy measurements. TD densities were dominated by edge-type TDs with screw-component TDs accounting for less than 10% of the total TD density. A significant decrease in edge-type TD density was observed for In-face InN films grown at increasingly higher substrate temperatures. In-face InN films grown with excess In exhibited lower TD densities compared to films grown under N-rich conditions. The edge-type TD density of N-face InN films was independent of substrate temperature due to the higher allowable growth temperatures for N-face InN compared to In-face InN. TD densities in In-face InN also showed a strong dependence on film thickness. Films grown at a thickness of less than 1 μm had higher TD densities compared with films grown thicker than 1 μm. The lowest measured TD density for an In-face InN film was $\sim 1.5\times 10^{10}/\text{cm}^2$ for 1 μm thick films.
© *2010 American Institute of Physics*. [doi:10.1063/1.3319557]

I. INTRODUCTION

It is well established that semiconductor film quality is an important issue in III-V device performance. Threading dislocation (TD) densities greater than $\sim 10^4$ cm^{-2} significantly decrease the efficiencies of GaP and GaAs based optoelectronic devices.[1–3] Fortunately, GaN optoelectronic devices perform reasonably well even with much higher TD densities (as high as 10^{10} cm^{-2}).[4] GaN-based devices, however, can be deleteriously impacted by TDs and a significant body of research has focused on decreasing the TD densities in these films to improve device performance.

The impact of TDs on device performance remains an area of ongoing research, however, there are many reports detailing some of the effects that TDs have on GaN. Rosner *et al.*[5] reported on cathodoluminescence inhomogeneity and decreased efficiency within the vicinity of TDs in bulk GaN films grown by MOCVD. The observations of decreased electron mobilities in *n*-type GaN films have been attributed to TD scattering.[6,7] Comprehensive transport models supporting the deleterious effects of TDs on electron mobilities confirm these observations,[8–10] and demonstrate the need to reduce TD densities for improved electronic performance of GaN-based devices. A similar research focus considering the effect of TDs on the electronic properties of InN has recently gained attention due to the improved epitaxial techniques for producing high-quality films.

It has been suggested that TDs with dangling bonds behave as donors in InN films and may be a significant source of the high electron concentration in unintentionally doped InN films.[11–13] The dominant unintentional donor in InN is highly disputed due to the prediction by Look *et al.*[14] that TDs in InN are negatively charged, similar to the direct observation of negatively charged TDs in bulk GaN.[15] Using the updated band gap value of ~ 0.7 eV, Piper *et al.*[11] more recently reported that the formation of positively charged nitrogen vacancies at the cores of TDs in InN are energetically favorable in the absence of impurities, suggesting that TDs are the dominant donor in InN. Lebedev *et al.*[12] used variable temperature Hall measurements to observe a relatively constant electron sheet density from room temperature to ~ 100 K, which was suggested as evidence for direct carrier generation from TDs. This is a contrasting viewpoint to the report by Thakur *et al.*[16] who established the need for negatively charged TDs in InN for charge balance and no correlation between TD densities and carrier concentrations was made.

Despite this lack of agreement about the effect TDs have on carrier concentrations in InN films, there is a consensus that TDs are the dominant scattering centers limiting the mobility of electrons in bulk InN. In 2002, Look *et al.*[14] first reported on the scattering of electrons by TDs in InN which was subsequently confirmed by several other groups.[12,16–18] Lebedev *et al.*[12] suggested TD strain scattering to be the dominant mechanism in limiting the mobility of electrons in InN. This claim was supported by Wang *et al.*[17] who predict a room temperature electron mobility in bulk InN of 10 000 cm^2/Vs with decreased TD densities. It should be noted that neither group dismissed the effects of additional scattering mechanisms such as neutral and charged impurity scattering or optical and acoustic phonon scattering, however, the TD scattering mechanism was far too dominant for any of these other mechanisms to be observed.[12,17]

The significant body of work considering TDs in InN and the general disagreement on the effect that TDs have on film properties indicates further understanding is needed. In this work, the origin of the TDs in InN films and the measurement techniques used to observe and evaluate the TDs will be discussed. The dependence of TD densities on film

[a]Electronic mail: chadsg@engineering.ucsb.edu.

 © 2010 American Institute of Physics

Downloaded 22 Nov 2010 to 129.187.254.46. Redistribution subject to AIP license or copyright; see http://jap.aip.org/about/rights_and_permissions

thickness and growth conditions in the context of the In-face InN growth diagram will be analyzed. Finally, a comparison to N-face InN will be presented.

II. EXPERIMENTS

To study the effect of growth conditions on the structural properties of InN, films were grown at varying substrate temperatures and In-fluxes while maintaining a constant active N-limited growth rate as described in our previous work.[19–21] The In-face InN samples presented here were grown in a Veeco 930 growth chamber and the N-face InN samples were grown in an Epi 620 growth chamber. Both growth systems used conventional Knudsen cells for group III sources and Veeco Uni-Bulb radio frequency plasma sources for the active N species. All of the In-face InN samples were grown on semi-insulating (Fe-doped) Ga-face GaN templates provided by Lumilog. The N-face InN films were deposited on free-standing N-face GaN provided by Lumilog. Homoepitaxially deposited GaN buffer layers preceded InN growth for both substrate orientations. The GaN buffer layers were grown using deposition conditions optimized for the smoothest GaN surface morphology to provide the flattest starting surface for InN growth. The GaN was deposited at 700 °C in the Ga-droplet regime and Ga-droplets were desorbed prior to InN growth.[19–22] An Ircon Modline 3 pyrometer was employed to measure the growth temperature. Reflection high energy electron diffraction (RHEED) was used to monitor the InN growth mode and In-metal coverage *in situ*.

The systematic study of the effect of growth conditions on InN structural quality is schematically represented in Fig. 1(a). In-face InN films were evaluated by measuring the rocking curve FWHM of samples grown at varying substrate temperatures and indium flux Φ_{In} while maintaining a constant active nitrogen flux Φ_N of 10.5 nm/min. For the In-face InN sample series, Φ_{In} was varied such that growth occurred in the In-droplet regime, the N-rich regime, and approximately on the crossover from N-rich growth to In-droplet growth (nominally stoichiometric growth conditions). Samples grown in the In-droplet regime had an excess impinging Φ_{In} of 2 nm/min and samples grown in the N-rich regime were deficient of 2 nm/min Φ_{In}. This precise control of Φ_{In} required adjustment of the In cell temperature for each substrate temperature due to increasing InN decomposition at higher substrate temperatures. The dependence of the TD density on InN film thickness was also explored. InN layers of varying thickness were grown in the In-droplet regime using the same substrate temperature (470 °C) and In-flux (corresponding to 2 nm/min excess In).

The N-face InN sample set [Fig. 1(b)] included samples grown with an excess Φ_{In} of 3 nm/min and samples grown with a deficient Φ_{In} of 2 nm/min. These samples were also evaluated by on-axis and off-axis x-ray rocking curves. The growth temperatures of the N-face InN were much higher than the In-face sample set in this analysis. The lowest N-face InN growth temperature considered was 500 °C—a growth temperature too high for In-face InN due to InN decomposition.

These films were then evaluated by high resolution x-ray

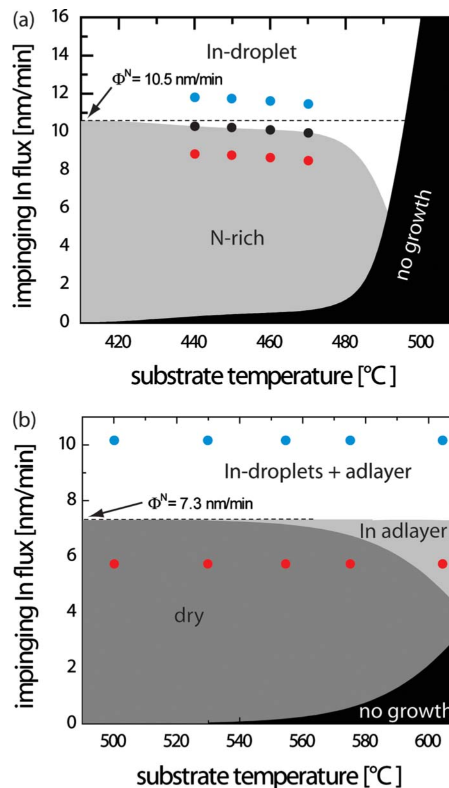

FIG. 1. (Color online) Schematic representations of the sample sets used to study the effect of growth conditions on the TD densities of InN films grown on GaN. (a) In-face InN samples were grown at different substrate temperatures varying only the Φ_{In} to establish In-droplet growth conditions (blue circles), stoichiometric growth conditions (black circles) and N-rich growth conditions (red circles). (b) N-face InN samples were grown at different substrate temperatures and two different Φ_{In} corresponding to growth in the In-droplet regime using the high flux (blue circles) and either dry growth or growth with an In adlayer using the low flux (red circles).

diffraction (HRXRD) in a panalytical materials research diffractometer PRO, providing a powerful and nondestructive method to evaluate the defect density in polar and nonpolar InN.[23,24] Full-width half-maximum (FWHM) values of InN ω-scan rocking curves were measured with an open detector in symmetric on-axis and skew-symmetric off-axis orientations. On-axis symmetric rocking curve FWHMs were measured for the (0002) basal plane—with a surface normal parallel to the growth direction. The off-axis, skew symmetric rocking curve FWHMs were measured for the $(10\bar{1}2)$ and $(20\bar{2}1)$ planes—oriented 43° and 75° from the (0001) film plane. The rocking curve FWHM values were then used to assess the TD densities of the InN films. Plan-view and cross-sectional transmission electron microscopy (TEM) was used to directly observe the TDs in select InN films.

III. RESULTS

The significant lattice mismatch between InN and GaN (9.6%) lead to InN growth following the Volmer–Weber growth mode in which strained three-dimensional InN islands first nucleated on GaN then relaxed after ~2.5 monolayers (ML) of InN deposition.[25] These islands then grew laterally until coalescence and a uniform InN film was formed. The Volmer–Weber growth mode, island coales-

Downloaded 22 Nov 2010 to 129.187.254.46. Redistribution subject to AIP license or copyright; see http://jap.aip.org/about/rights_and_permissions

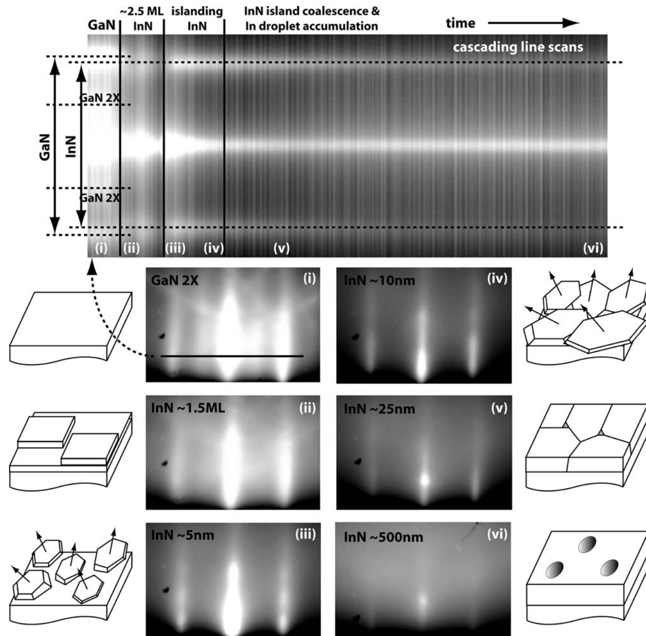

FIG. 2. Cascading RHEED line scans (top) depicting the RHEED intensity and surface reconstructions at the onset of InN growth. The RHEED images [(i)-(vi)] indicate surface roughness and metal coverage at various points during InN deposition. (i) The dry GaN surface just before InN deposition. (ii) The initial In-adlayer accumulation during InN growth. (iii) InN islanding (VW growth mode) begins with crystallites slightly misoriented. (iv) InN islands beginning to coalesce. (v) Island coalescence essentially completed and a coherent InN film had formed. Slight pitting has occurred and dislocations are generated at coalescence boundaries. (vi) Fully coherent InN film with metallic In droplet accumulation on the InN surface.

cence, and subsequent In-droplet formation during In-rich growth was observable in the RHEED patterns. Figure 2 shows representative RHEED patterns and corresponding schematic representations illustrating the evolution of the surface at the onset of In-rich InN growth at a substrate temperature of 470 °C.

The cascading RHEED line scans (Fig. 2) show the initial 2×2 dry GaN surface reconstruction [also in the RHEED image labeled (i)] evolved into the InN surface reconstruction [RHEED images (ii)-(vi)]. During the first ~2.5 ML the RHEED pattern remained smooth [Fig. 2(ii)] and the RHEED intensity oscillated 2.5 times. These initial intensity oscillations were due to metallic In-adlayer accumulation during the initial stage of In-rich growth—described in more detail elsewhere.[20] Once the InN thickness exceeded ~2.5 ML, the RHEED patterns began to exhibit spottiness along the surface reconstruction lines [Figs. 2(iii) and 2(iv)] indicative of a three-dimensional/islandlike growth mode. Upon further InN growth, the RHEED pattern became smooth again as the InN film coalesced [Fig. 2(v)]. As the film growth continued the RHEED intensity decreased significantly [Fig. 2(vi)], indicative of metallic In accumulation on the InN surface.[26,27]

Similar to the TD structure observed in (0001) GaN growth on sapphire,[28–31] three TD types arise from this island coalescence: screw-type TDs (Burgers vector $\mathbf{b}=\pm\mathbf{c}$ where $\mathbf{c}$ is the c-axis translation vector), edge-type TDs [$\mathbf{b}=\pm\mathbf{a}_i$ ($i=1,2,3$) where $\mathbf{a}_i$ is the lattice translation vector and equals $\pm\frac{1}{3}\langle 11\bar{2}0\rangle$] and TDs with mixed character [$\mathbf{b}=\pm(\mathbf{a}_i\pm c)$]. These TDs can be directly observed by TEM or inferred from interpretation of x-ray rocking curve (ω-scans) FWHM values in a mosaic block model. Since the x-ray measurement is nondestructive and takes significantly less time than the TEM measurement, ω-scans are the preferred method for evaluating TD densities in InN grown on GaN. Understanding the effect of these TDs on rocking curve FWHM's is the first step in evaluating the structural quality of the InN films.

The InN mosaic blocks, also referred to as subgrains or crystallites, that form due to the islandlike nature of the growth can be misoriented with respect to the underlying GaN in two relevant ways: (i) *tilted*, as defined by the crystallite surface normal being nonparallel to the substrate surface normal (schematically illustrated in Fig. 2 by the InN crystallite surface normals), and (ii) *twisted*, as defined by the crystallite being rotated in the basal plane relative to the substrate.[31] In (0001) oriented group III nitrides, TDs typically have line direction parallel to the [0001] direction. Tilt is related to TDs with a Burgers vector component parallel to the film surface normal. In coalesced films, tilt is sustained by TDs with a Burger's vector component parallel to the c-axis, i.e., via either pure screw or mixed character TDs.[31] The strain fields from the screw-component TDs distort the on-axis (000l) planes and, therefore, broaden on-axis rocking curves measurements.[29] Conversely, twist in the InN mosaic is realized by TDs with an in-plane component of the Burgers vector.[31] Pure edge-type TDs and TDs with edge-type TD character fall in this category.[29,31] When measured in a skew symmetric geometry, off-axis planes are disrupted by edge type TDs and the FWHM of skew symmetric rocking curves, such as $(10\bar{1}2)$ and $(20\bar{2}1)$, are broadened by the presence of such TDs.[29,31,32]

Figure 3(a) shows an HRXRD $\omega/2\theta$ scan for a typical 1 μm InN layer grown on a GaN substrate. The (0002) InN peak is separated from the underlying GaN (0002) peak indicating a fully relaxed InN film (confirmed by HRXRD reciprocal space mapping of the sample). The data in Fig. 3(b) shows representative data of the three rocking curves discussed above used to evaluate the structural quality of InN films. The on-axis, symmetric (0002) rocking curve FWHM is much narrower than either of the FWHMs of the two off-axis skew symmetric reflections. This is indicative of a TD structure dominated by edge-type TDs which is analogous to the dislocation network observed in GaN growth on sapphire.[29]

The TD character was more closely analyzed by cross-sectional TEM. Figure 4 shows two cross-sectional TEM images recorded in two-beam conditions for imaging pure edge-type TDs [Fig. 4(a) $g=(1\bar{1}00)$] and screw-component TDs [Fig. 4(b) $g=(0002)$]. The TEM micrographs confirmed the XRD data that edge-type TDs were the dominant TD in the InN film. The total TD density in this film as determined by plan view TEM [shown in Fig. 5(a)] was 3×10^{10} cm^{-2}. The density of TDs with screw-component character was 3×10^{8} cm^{-2}—two orders of magnitude less than the density of edge-type TDs; therefore, the overall TD density can be approximated by determining the density of edge-type TDs.

Downloaded 22 Nov 2010 to 129.187.254.46. Redistribution subject to AIP license or copyright; see http://jap.aip.org/about/rights_and_permissions

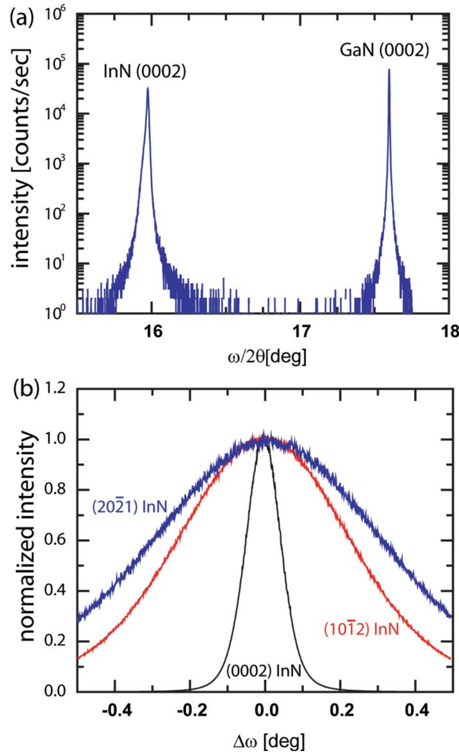

FIG. 3. (Color online) Representative XRD data for a 1 μm InN sample. (a) The $\omega/2\theta$ scan showing a fully relaxed InN film on the underlying GaN film. (b) Symmetric on-axis (0002) (black curve) and skew symmetric off-axis (10$\bar{1}$2) (red curve) and (20$\bar{2}$1) (blue curve) rocking curves for the same 1 μm InN sample shown in (a).

The TD densities in InN films were also calculated using the FWHM data from the on-(symmetric) and two off-axis (skew symmetric) rocking curves. The models developed by Srikant *et al.*[31] for the evaluation on x-ray rocking curves in large mosaic films and applied specifically to GaN by Lee *et al.*[32] were used determined the calculations described here.

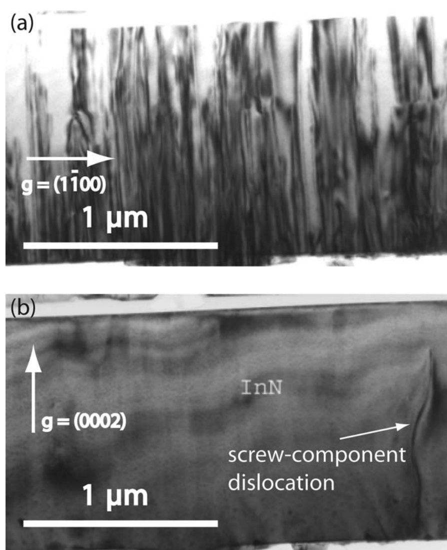

FIG. 4. Cross-sectional TEM micrographs of a 1.5 μm InN film grown on GaN. (a) g=(1$\bar{1}$00) image—showing pure edge-type TDs and (b) g =(0002) image—showing a single screw-component TD. These images provide additional evidence that the TD structure of InN on GaN is dominated by edge-type TDs.

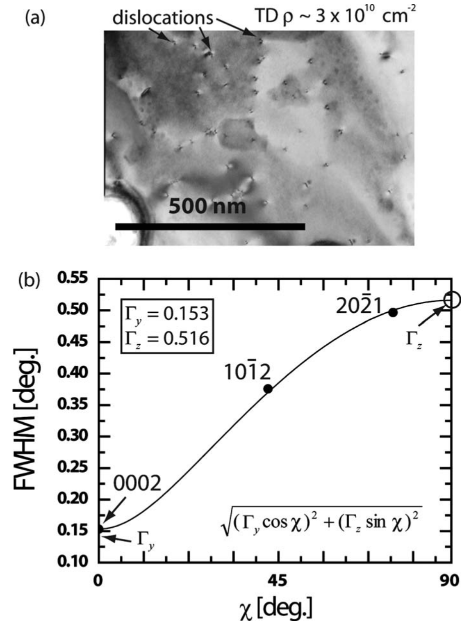

FIG. 5. (a) Plan-view TEM of the InN sample from showing an overall threading dislocation density of $\sim 3\times 10^{10}$ cm^{-2}. (b) Resulting curve of Eq. (1) using the FWHM values from the rocking curves shown in Fig. 3. A twist angle of 0.516° was determined by extrapolating the FWHM values of increasingly off-axis rocking curves.

By extrapolating the FWHM values of the increasingly off-axis rocking curves to 90° (with the on-axis rocking curve at 0° defined as the tilt angle—Γ_y), according to Eq. (1) (from Refs. 31 and 32), a value for the twist angle (Γ_z) was determined. Figure 5(b) depicts the resulting curve from Eq. (1) for the InN sample with the corresponding plan-view TEM micrograph shown in Fig. 5(a).

$$\Gamma = \sqrt{(\Gamma_y \cos \chi)^2 + (\Gamma_z \sin \chi)^2}, \tag{1}$$

where Γ is the FWHM at an inclination angle χ of the Bragg plane from the normal (0002) orientation, Γ_y (the tilt angle) is the on-axis (0002) rocking curve FWHM and Γ_z (the twist angle) is the extrapolated FWHM value for a rocking curve rotated 90° to the surface normal.

The resulting angles can then be used to calculate the TD densities with screw character (using the tilt angle, Γ_y) and with pure edge character (using the twist angle, Γ_z) according to Eqs. (2) and (3).[31,32] These equations were derived from several classic formulae[33–35] and applied to the GaN system by Lee *et al.*[32]

$$\rho_s = \Gamma_y^2/1.88c^2, \tag{2}$$

$$\rho_e = \Gamma_z^2/1.88a^2. \tag{3}$$

In which ρ_s and ρ_e are the screw and edge TD densities, c and a are the relevant Burgers vectors (the InN c lattice constant of 5.693 Å for TDs with screw character and the InN a lattice constant of 3.533 Å for pure edge TDs), and 1.88 is a TEM calibration constant determined for GaN and extrapolated to InN for our purposes. The calculated density of TDs with screw character for the sample shown in Fig. 4 is 1.1×10^9 cm^{-2} and the calculated density of pure edge-type TDs is 3.5×10^{10} cm^{-2}, in good agreement with the

Downloaded 22 Nov 2010 to 129.187.254.46. Redistribution subject to AIP license or copyright; see http://jap.aip.org/about/rights_and_permissions

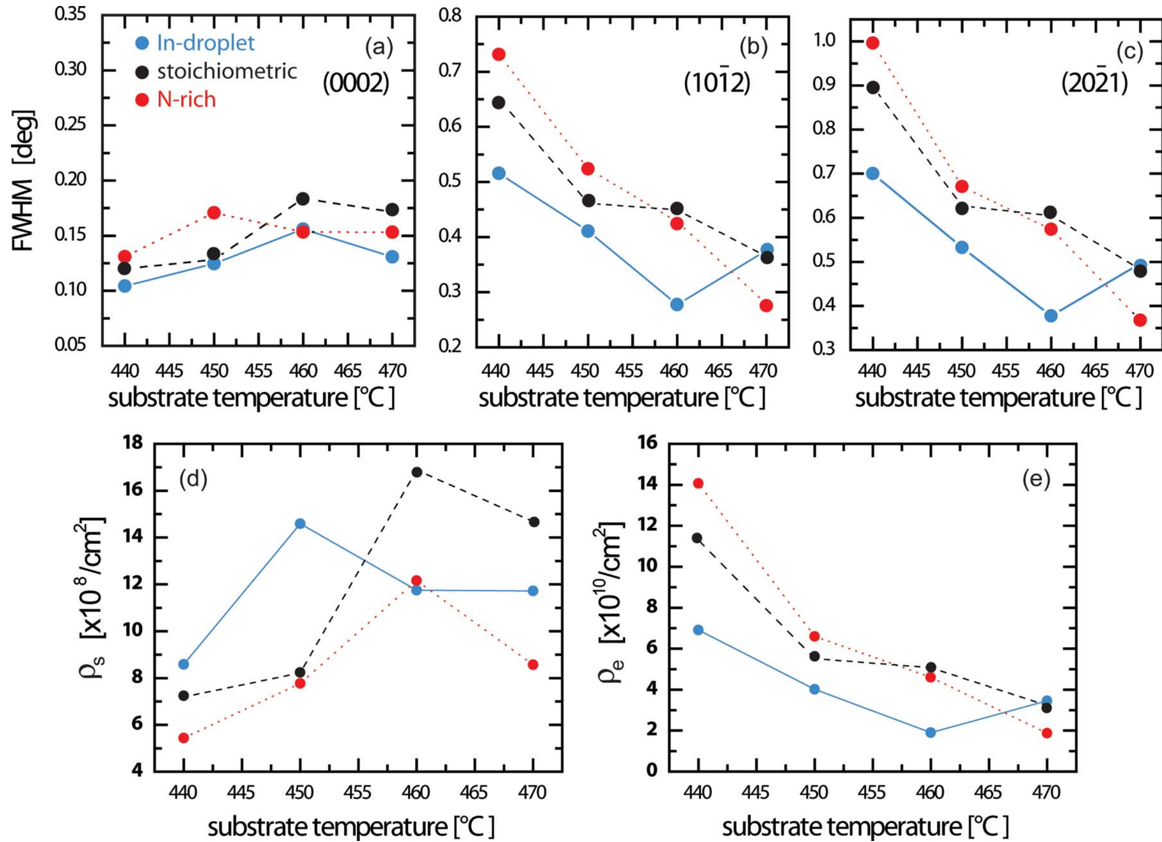

FIG. 6. (Color online) Measured (XRD) and calculated (TD densities) data for the sample set used to study the effect of growth conditions on the structural quality of In-face InN. InN samples were grown at different substrate temperatures varying only the Φ_{In} to establish In-droplet growth conditions (blue circles), stoichiometric growth conditions (black circles with dashed lines) and N-rich growth conditions (red circles with dotted lines) (a) FWHM values of the symmetric on-axis (0002) x-ray rocking curves. [(b) and (c)] FWHM values of the skew symmetric off-axis (10$\bar{1}$2) and (20$\bar{2}$1) x-ray rocking curves. (d) Calculated densities of TDs with screw character using Eq. (2) and the on-axis (tilt) FWHM values from (a). (e) Calculated pure edge-type TD densities using Eq. (3) and extrapolated twist angles using the XRD data from [(a)-(c)]. The *y*-axis scale for the screw component TD density data is two orders of magnitude less than the scale for the edge-type TD data.

observed TEM data. This calculation was used to determine TD densities in InN films throughout the rest of this work.

The screw component TDs accounted for only 3% of the total TD density in this representative In-face InN film which is similar to the case of GaN on sapphire where the screw component TD density typically ranges from 1% to 20% of the total TD density depending on the growth method and nucleation procedure.[36]

Figure 6 shows the on-axis and off-axis x-ray rocking curve results and the calculated TD densities. The FWHM values of on-axis, symmetric rocking curves [Fig. 6(a)] and the calculated screw component TD densities [Fig. 6(d)] show the relative insensitivity of screw component TDs to growth temperature across all growth regimes. This data also indicates that samples grown in the In-droplet regime have slightly lower screw-component TD densities than samples grown N-rich or under stoichiometric conditions. The FWHM values of the off-axis, skew symmetric rocking curves [Figs. 6(b) and 6(c)] decrease at increasing growth temperatures for all three growth regimes with the In-droplet samples exhibiting the lowest values. The calculated pure edge-type TD densities decrease correspondingly at higher growth temperatures [Fig. 6(e)].

The decreased edge-type TD densities at higher substrate temperatures can be explained by considering the effect of substrate temperature at the onset of InN deposition. The island nucleation and subsequent film coalescence (discussed previously) leads to coalescence boundaries in the form of edge-type TDs. Presumably at higher growth temperatures, the InN three-dimensional island density decreased due to a decrease in driving force for growth and as a result there were fewer coalescence boundaries (edge-type TDs) as the islands formed the planar epitaxial film.

The lower edge-type TD density for InN films grown with excess In can also be understood by considering the behavior of island coalescence when a complete InN film forms. The observed metallic In-adlayer during In-droplet InN growth increases adatom mobility leading to morphologically smoother films.[20,37] The increased adatom mobility due to the presence of the In-adlayer also leads to enhanced lateral island growth and a large island size at island coalescence. Presumably the larger islands, on average, have improved alignment with respect to the underlying GaN and thus the mosaic is reduced for larger island size—in fact this is the only reasonable explanation for reduced rocking curve widths for larger island size at coalescence. Therefore, films grown with excess In have fewer edge-type TDs than films grown in the N-rich regime at the same substrate temperature.

The dependence of the calculated TD densities on thick-

Downloaded 22 Nov 2010 to 129.187.254.46. Redistribution subject to AIP license or copyright; see http://jap.aip.org/about/rights_and_permissions

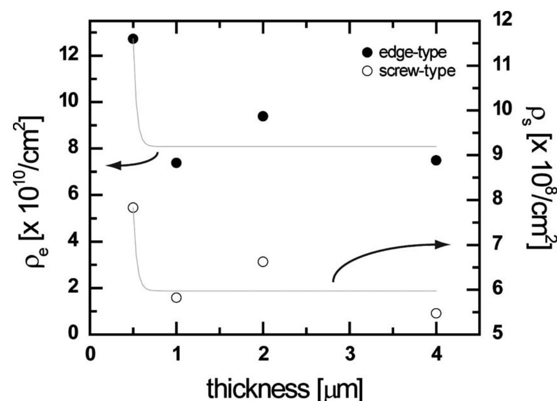

FIG. 7. TD dependence on thickness of In-face InN. The open circles represent the density of TDs with screw character and the filled black circles represent the pure edge-type TD density. The light gray curves are guides to the eye.

ness is shown in Fig. 7. Pure edge-type TDs dominated the overall TD density for all thicknesses. InN films grown 1 μm and thicker exhibited a roughly constant TD density; in the range of 7×10^{10}–9×10^{10} cm^{-2}. Films grown less than 1 μm thick had significantly higher TD densities. The 500 nm thick sample from Fig. 7 had a TD density of 1.3 $\times10^{11}$ cm^{-2} and InN films thinner than 500 nm (not shown in Fig. 7 due to differences in growth conditions) exhibited even higher TD densities.

The reduction of TDs in InN films over 1 μm thick compared to films thinner than 1 μm suggested that TD annihilation was complete at a thickness between 0.5 μm and 1 μm. This observation is similar to Lebedev *et al.*[38] who used TEM analysis of a thick InN film to measure TD densities. They observed an exponential decay of TD densities with film thickness that reached an asymptotic limit around 1 μm.[38]

A comparison of the effect of growth conditions on TD densities for both In- and N-face InN included the In-face sample set described above. The resulting pure edge-type TD densities for both In- and N-face InN are shown in Fig. 8. The minority screw-component TDs are not shown since they represent only a small fraction of the total TD density. The decrease of TDs observed with increasing growth temperature and Φ_{In} for the In-face InN sample set [Fig. 8(a)] was not observed for N-face InN films [Fig. 8(b)]. Increased

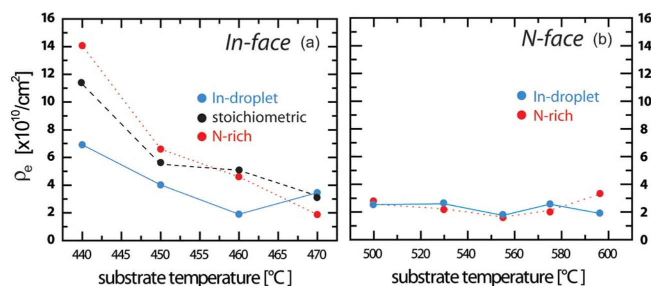

FIG. 8. (Color online) (a) Dependence of In-face InN edge-type TD density dependence on substrate temperature and Φ_{In} (repeated from Fig. 6(e)). (b) Dependence of N-face InN edge-type TD density on growth temperature and growth regime. The same *y*-axis scale is used in both cases to illustrate the relative insensitivity of the TD density on substrate temperature for the N-face case.

Φ_{In} had a small effect on the TD density at only the highest growth temperature. We have also grown N-face InN films on GaN buffer layers on C–face SiC substrates (not shown here) and noticed no differences in TD densities as compared to direct growth on free–standing N-face GaN substrates. This indicates that the mismatch with the GaN buffer layer determines the density of TDs.

The insensitivity of TD density on growth conditions for N-face InN was in contrast with other reports on N-face InN[39] and to the effect that growth conditions had on In-face InN. The lower growth temperatures necessary for In-face InN growth likely resulted in lower adatom mobility during growth than for the N-face InN samples grown at higher temperatures. Slower adatom mobility provided an environment for a higher island density during the Volmer–Weber growth mode for the In-face samples than the N-face samples. The higher adatom mobility during the N-face InN growth also provided faster lateral island growth and quicker island coalescence compared to In-face InN. The island coalescence boundaries were fewer for N-face than In-face InN creating fewer TDs in N-face InN films for the typical growth temperatures. There are also interesting differences in terms of In adlayer mediated adatom mobilities, i.e., while the 2.5 ML thick In adlayer[20] plays a large role in edge–type TD for In–face InN, the 1-ML-thick In adlayer on N-face InN[21] is nearly insignificant. This corroborates further the fact that growth temperature is the dominant parameter determining variations in edge-type TD densities in c–plane InN.

IV. CONCLUSIONS

The dependence of TD densities on InN polarity and growth conditions has been presented. For both In- and N-face InN, pure edge-type TDs dominated the TD structure and screw-component TDs accounted for only 1%–5% of the total TD density. TDs were shown to asymptotically reach a minimum value by a thickness of 1 μm in In-face InN. TD densities in In-face InN depended on both the growth regime and growth temperature, whereas, TDs in N-face InN films showed minimal dependence on typical growth conditions. For In-face InN, the optimum growth conditions for minimizing the TD density were shown to scale with excess In at high substrate temperatures. Optimal In-face InN growth conditions then include a substrate temperature of 470 °C in the In-droplet regime to achieve minimum TD densities.

ACKNOWLEDGMENTS

This work was supported by AFOSR (Award No. FA9550–08–1–0461, Kitt Reinhardt program manager). This work made use of the Central Facilities supported by the NSF MRSEC program under Award No. DMR05–20415. We would like to acknowledge Chris van de Walle, Umesh Mishra, and Arthur Gossard for useful discussions.

[1]A. H. Herzog, D. L. Keune, and M. G. Craford, J. Appl. Phys. **43**, 600 (1972).
[2]R. J. Roedel, A. R. V. Neida, R. Caruso, and L. R. Dawson, J. Electrochem. Soc. **126**, 637 (1979).
[3]W. A. Brantley, O. G. Lorimor, P. D. Dapkus, S. E. Haszko, and R. H.

Downloaded 22 Nov 2010 to 129.187.254.46. Redistribution subject to AIP license or copyright; see http://jap.aip.org/about/rights_and_permissions

Saul, J. Appl. Phys. **46**, 2629 (1975).
[4]S. D. Lester, F. A. Ponce, M. G. Craford, and D. A. Steigerwald, Appl. Phys. Lett. **66**, 1249 (1995).
[5]S. J. Rosner, E. C. Carr, M. J. Ludowise, G. Girolami, and H. I. Erikson, Appl. Phys. Lett. **70**, 420 (1997).
[6]N. G. Weimann, L. F. Eastman, D. Doppalapudi, H. M. Ng, and T. D. Moustakas, J. Appl. Phys. **83**, 3656 (1998).
[7]H. M. Ng, D. Doppalapudi, T. D. Moustakas, N. G. Weimann, and L. F. Eastman, Appl. Phys. Lett. **73**, 821 (1998).
[8]D. Jena, Phys. Rev. B **70**, 245203 (2004).
[9]H. Tang, J. Webb, J. Bardwell, B. Leathem, S. Charbonneau, and S. Raymond, J. Electron. Mater. **29**, 268 (2000).
[10]D. C. Look and J. R. Sizelove, Phys. Rev. Lett. **82**, 1237 (1999).
[11]L. F. J. Piper, T. D. Veal, C. F. McConville, L. Hai, and W. J. Schaff, Appl. Phys. Lett. **88**, 252109 (2006).
[12]V. Lebedev, V. Cimalla, T. Baumann, O. Ambacher, F. M. Morales, J. G. Lozano, and D. Gonzalez, J. Appl. Phys. **100**, 094903 (2006).
[13]X. Wang, S.-B. Che, Y. Ishitani, and A. Yoshikawa, Appl. Phys. Lett. **90**, 151901 (2007).
[14]D. C. Look, H. Lu, W. J. Schaff, J. Jasinski, and Z. Liliental-Weber, Appl. Phys. Lett. **80**, 258 (2002).
[15]P. J. Hansen, Y. E. Strausser, A. N. Erickson, E. J. Tarsa, P. Kozodoy, E. G. Brazel, J. P. Ibbetson, U. Mishra, V. Narayanamurti, S. P. DenBaars, and J. S. Speck, Appl. Phys. Lett. **72**, 2247 (1998).
[16]J. S. Thakur, R. Naik, V. M. Naik, D. Haddad, G. W. Auner, H. Lu, and W. J. Schaff, J. Appl. Phys. **99**, 023504 (2006).
[17]K. Wang, Y. Cao, J. Simon, J. Zhang, A. Mintairov, J. Merz, D. Hall, T. Kosel, and D. Jena, Appl. Phys. Lett. **89**, 162110 (2006).
[18]C. S. Gallinat, G. Koblmüller, and J. S. Speck, Appl. Phys. Lett. **95**, 022103 (2009).
[19]C. S. Gallinat, G. Koblmüller, J. S. Brown, S. Bernardis, J. S. Speck, G. D. Chern, E. D. Readinger, H. Shen, and M. Wraback, Appl. Phys. Lett. **89**, 032109 (2006).
[20]C. S. Gallinat, G. Koblmüller, J. S. Brown, and J. S. Speck, J. Appl. Phys. **102**, 064907 (2007).
[21]G. Koblmüller, C. S. Gallinat, and J. S. Speck, J. Appl. Phys. **101**, 083516 (2007).
[22]G. Koblmüller, C. S. Gallinat, S. Bernardis, J. S. Speck, G. D. Chern, E. D. Readinger, H. Shen, and M. Wraback, Appl. Phys. Lett. **89**, 071902 (2006).
[23]G. Koblmüller, G. D. Metcalfe, M. Wraback, F. Wu, C. S. Gallinat, and J. S. Speck, Appl. Phys. Lett. **94**, 091905 (2009).
[24]G. Koblmüller, A. Hirai, F. Wu, C. S. Gallinat, G. D. Metcalfe, H. Shen, M. Wraback, and J. S. Speck, Appl. Phys. Lett. **93**, 171902 (2008).
[25]Y. F. Ng, Y. G. Cao, M. H. Xie, X. L. Wang, and S. Y. Tong, Appl. Phys. Lett. **81**, 3960 (2002).
[26]E. J. Tarsa, B. Heying, X. H. Wu, P. Fini, S. P. DenBaars, and J. S. Speck, J. Appl. Phys. **82**, 5472 (1997).
[27]C. Adelmann, J. Brault, D. Jalabert, P. Gentile, H. Mariette, G. Mula, and B. Daudin, J. Appl. Phys. **91**, 9638 (2002).
[28]X. H. Wu, P. Fini, E. J. Tarsa, B. Heying, S. Keller, U. K. Mishra, S. P. DenBaars, and J. S. Speck, J. Cryst. Growth **189–190**, 231 (1998).
[29]B. Heying, X. H. Wu, S. Keller, Y. Li, D. Kapolnek, B. P. Keller, S. P. DenBaars, and J. S. Speck, Appl. Phys. Lett. **68**, 643 (1996).
[30]W. Qian, M. Skowronski, M. D. Graef, K. Doverspike, L. B. Rowland, and D. K. Gaskill, Appl. Phys. Lett. **66**, 1252 (1995).
[31]V. Srikant, J. S. Speck, and D. R. Clarke, J. Appl. Phys. **82**, 4286 (1997).
[32]S. R. Lee, A. M. West, A. A. Allerman, K. E. Waldrip, D. M. Follstaedt, P. P. Provencio, D. D. Koleske, and C. R. Abernathy, Appl. Phys. Lett. **86**, 241904 (2005).
[33]M. J. Hordon and B. L. Averbach, Acta Metall. **9**, 237 (1961).
[34]C. G. Dunn and E. F. Kogh, Acta Metall. **5**, 548 (1957).
[35]P. Gay, P. B. Hirsch, and A. Kelly, Acta Metall. **1**, 315 (1953).
[36]S. K. Mathis, A. E. Romanov, L. F. Chen, G. E. Beltz, W. Pompe, and J. S. Speck, Phys. Status Solidi A **179**, 125 (2000).
[37]G. Koblmüller, S. Fernandez-Garrido, E. Calleja, and J. S. Speck, Appl. Phys. Lett. **91**, 161904 (2007).
[38]V. Lebedev, V. Cimalla, J. Pezoldt, M. Himmerlich, S. Krischok, J. A. Schaefer, O. Ambacher, F. M. Morales, J. G. Lozano, and D. Gonzalez, J. Appl. Phys. **100**, 094902 (2006).
[39]X. Wang, S.-B. Che, Y. Ishitani, and A. Yoshikawa, Phys. Status Solidi B **243**, 1456 (2006).

Downloaded 22 Nov 2010 to 129.187.254.46. Redistribution subject to AIP license or copyright; see http://jap.aip.org/about/rights_and_permissions